# Seasonal methane accumulation and release from a gas emission site in the central North Sea

S. Mau[1]*, T. Gentz[2], J.-H. Körber[1], M. E. Torres[3], M. Römer[1], H. Sahling[1], P. Wintersteller[1], R. Martinez[2], M. Schlüter[2], E. Helmke[2]

[1] MARUM – Center for Marine Environmental Sciences and Department of Geosciences, University of Bremen, Klagenfurter Str., 28359 Bremen, Germany

[2] Alfred Wegener Institute Helmholtz Centre for Polar and Marine Research, Am Handelshafen 12, 27570 Bremerhaven, Germany

[3] College of Oceanic and Atmospheric Sciences, Oregon State University, 104 Ocean Admin Building, Corvallis, Oregon 97331-5503

* Corresponding author: Susan Mau, e-mail: smau@marum.de

Abstract

We investigated dissolved methane distributions along a 6 km transect crossing active seep sites at 40 m water depth in the central North Sea. These investigations were done under conditions of thermal stratification in summer (July 2013) and homogenous water column in winter (January 2014). Dissolved methane accumulated below the seasonal thermocline in summer with a median concentration of 390 nM, whereas during winter, methane concentrations were typically much lower (median concentration of 22 nM). High resolution methane analysis using an underwater mass-spectrometer confirmed our summer results and were used to document prevailing stratification over the tidal cycle. We contrast estimates of methane oxidation rates (from 0.1 to 4.0 nM $day^{-1}$) using the traditional approach scaled to methane concentrations with microbial turnover time values, and suggest that the scaling to concentration may obscure the ecosystem microbial activity when comparing systems with different methane concentrations. Our measured and averaged rate constants (*k'*) were on the order of 0.01 $day^{-1}$, equivalent to a turnover time of 100 days, even when summer stratification led to enhanced methane concentrations in the bottom water. Consistent with these observations, we could not detect known methanotrophs and *pmoA*-genes in water samples collected during both seasons. Estimated methane fluxes indicate that horizontal transport is the dominant process dispersing the methane plume. During periods of high wind speed (winter), more methane is lost to the atmosphere than oxidized in the water. Microbial oxidation seems of minor importance throughout the year.

## 1 Introduction

Methane is, after water vapor and $CO_2$, the most important greenhouse gas. Its concentration has increased by a factor of 2.5 since preindustrial times, from 722 ppb in 1750 to 1800 ppb in 2011 (IPCC, 2013). The total global emission has been estimated to be ~550 Tg (methane) $yr^{-1}$ with an anthropogenic contribution of 50 to 65%. Geological sources, which were not considered in IPCC reports previously, are suggested to account for up to 30% of total emissions. These include anthropogenic emissions related to leaks in the fossil fuel industry, as well as natural geological seeps both terrestrial and marine (IPCC, 2013). An improved emission estimate from marine seeps suggests that these sources contribute ~20 Tg methane $yr^{-1}$, i.e., 4% of the global emissions, to the atmospheric methane (Etiope et al., 2008).

In general, oceans are a minor source of methane to the atmosphere, accounting for 2-10% of the global emissions (Bange et al., 1994). The main oceanic source (75%) is thought to originate from estuarine, shelf and coastal areas (Bange, 2006; Bange et al., 1994). The European coastal areas were found to emit 0.46-1 Tg $yr^{-1}$, but this value may underestimate the coastal input, since fluxes from estuaries and shallow seeps have not been represented adequately (Bange, 2006).

Although continental margins account for only 10% of the total ocean area and 20% of the marine primary production (Killops and Killops, 1993), more than 90% of all organic carbon burial occurs in sediments deposits on deltas, continental shelves, and upper continental slopes (Berner, 1989). At these locations, which also are characterized by high sedimentation rates, organic carbon is rapidly buried beneath the sulfate reduction zone and becomes available to methanogens (e.g. Cicerone and Oremland, 1988). Methane is also generated by thermal breakdown at high temperature and pressure. A significant fraction of the methane is oxidized in anaerobic and aerobic sediments (e.g. Boetius et al., 2000; Jørgensen and Kasten, 2006; King, 1992; Niewöhner et al., 1998). At cold seep sites, methane escaping microbial oxidation may be transported into the overlying water either dissolved in upwardly advecting pore waters or, in case of oversaturation, in the form of gas bubbles. Because methane is undersaturated in seawater, rising methane bubbles partially dissolve during ascent through the water column (McGinnis et al., 2006), where the dissolved methane may be further consumed by microbial oxidation. Only if this methane survives transport to the mixed layer, it may be transferred to the atmosphere.

Because of processes consuming methane in the water column, shallow seeps are more likely to contribute to the atmospheric methane pool. However, even at shallow sites, density stratification may limit vertical transport. For example, at the 70 m deep Tommeliten area in the North Sea, a summer thermocline constrains methane transport to the atmosphere and numerical modeling

showed that during this season less than ~4% of the gas initially released at the seafloor reaches the mixed layer (Schneider von Deimling et al., 2011). Here we examine the seasonal cycle of methane in the North Sea by chemical and microbiological analyses of water samples collected in a region of shallow seepage during summer (July 2013) and winter (January 2014). For the case of expected seasonal stratification; we further consider whether the methane trapped in bottom waters is significantly consumed by microbial oxidation during summer, thus limiting the fraction that can be released at the onset of storm events in fall.

### 1.1 Study Site

The study site is situated in an area of active gas venting above a shallow gas reservoir in the central North Sea south of Dogger Bank, a sandbank that is 20 m shallower than the surrounding seabed (Fig. 1). The gas vents are located in the Netherlands sector, license block B13 in a shallow (< 45 m) and flat region that lacks any morphological expression typical of seep structures (Schroot et al., 2005). The seeps are likely sourced from a biogenic methane reservoir ($\delta^{13}C$ values of -80‰ VPDB) of Pliocene to Pleistocene age, which lies 600-700 m below the seafloor. Schroot et al. (2005) imaged patches of gas-saturated sediments between the gas reservoir and the seafloor in seismic surveys. These data, plus observations of discreet bubble streams in the water column and rapidly decreasing methane concentrations in cores with distance from the vent site, led Schroot et al. (2005) to describe our study area as a leaking gas reservoir with laterally discontinuous seepage.

In this region, water masses from the north (Atlantic Water) and south (Straits of Dover) meet (Kröncke and Knust, 1995) and the general anticlockwise circulation along the coasts of the North Sea becomes weak and varied (Fig. 1, Howarth, 2001). Tides have the strongest influence on the currents in this region, with wind forcing becoming secondary (Howarth, 2001; Otto et al., 1990; Sündermann and Pohlmann, 2011).

Seasonal temperature stratification, common to this and other shelf seas, separates high-light and low-nutrient surface water from low-light and high-nutrient bottom water. Even though in some shelf areas, the tidal energy is sufficient to overcome stratification, Pingree and Griffiths (1978) and Holt and Umlauf (2008) have shown that our study area is situated east of the tidal front that bifurcates Dogger bank. Consequently, the water column above the Dogger sandbank is well-mixed throughout the year, whereas the deeper waters that surround the bank become stratified during spring and summer through the course of a tidal cycle.

## 2 Methods

All data used in this study was collected during two cruises with *RV Heincke*. The first cruise (HE406) was conducted during summer 2013 (20.-24. July), the second cruise (HE413) during winter 2014 (13.-22. January).

### 2.1 EM710 flare imaging

Hydroacoustic data was collected only during the winter cruise, using a Kongsberg EM710 multibeam echosounder to map active gas emissions (Fig. 2). For the precise localization of individual flares, i.e., bubble streams in an echogram, the water column data were post-processed using the Fledermaus tools FMMidwater, DMagic, and the 3D Editor (© QPS). The origin of individual flares was identified as the point of highest amplitudes near the seafloor. The coordinates of these points were extracted using the FMGeopicker and subsequently plotted on top of the bathymetry using ArcGIS 10.2 (©ESRI).

For visualization of flare deflections and bubble rising heights, selected flares were extracted from the water column data as point data and edited using the 3DEditor of DMagic. The processed flares were plotted over the bathymetry data in a 3D-view (Fig. 2).

### 2.2 Water column sampling

To identify the size and magnitude of the dissolved methane plume generated by the bubble discharge, seawater was sampled along a hydrocast transect that crossed the active gas emission sites (Fig. 2). The transect extends 3 km to the east and 3 km to the west from the main bubbling location denoted as cluster 1 in Fig. 2A and 2C (4°5.44'N, 55°18.36'E). To better capture the methane plumes and minimize tidal current changes, the station transect was oriented in the direction of the dominant E-W tidal water movement. The stations were sampled both in summer 2013 and in winter 2014; in both cases, the eastern sector (5 stations) was sampled on one day (~3 h) and the western sector (5 stations) on another day (~3 h), so that the station directly above cluster 1 was sampled twice.

We used a rosette equipped with twelve 5 L Niskin bottles mounted on a frame that holds a Sea-Bird SBE 911 plus CTD, and an SBE 43 oxygen sensor for online monitoring of salinity, temperature, pressure, and dissolved oxygen. The data are archived in PANGAEA (doi:10.1594 / PANGAEA.824863 and doi:10.1594 / PANGAEA.832334). Twelve different water depths were sampled at each station for quantification of the methane concentration and 5 water depths for methane oxidation rates. Additional casts were conducted to recover sufficient water for molecular analyses.

### 2.2.1 Methane concentration

For methane concentration analysis, samples were collected in 60 ml crimp-top glass bottles, flushed with 2 volumes of sample water and filled completely to eliminate bubbles. Bottles were immediately capped with butyl rubber stoppers and crimp sealed. After adding 0.2 ml of 10 M NaOH to stop any microbial activity, a 5 ml headspace of pure $N_2$ was introduced into each bottle as described in Valentine et al. (2001) and the samples were stored at 4 °C. One to two aliquots of the headspace were analyzed to determine methane concentrations using a gas-phase chromatograph equipped with a flame ionization detector. The methane concentrations were calculated as detailed in Magen et al. (2014). Analyses were performed both on board and post cruise. Replicate analyses of samples yielded a precision of ± 5%.

### 2.2.2 Methane oxidation rates

Methane oxidation (MOx) rates were determined from ex situ incubations of water samples in 100 ml serum vials. Sample collection and incubation were performed as described in Mau et al. (2013). Briefly, duplicate samples were collected and 50 µl of $^3$H-labeled methane (160–210 kBq) in $N_2$ were added to each sample. After shaking the bottles to equilibrate the tracer with the water, the samples were incubated in the dark for 24 h, those collected in summer 2013 were incubated at 10 °C and those from winter 2014 at 9 °C. After incubation, the total activity ($^3$H-$CH_4$ + $^3$H-$H_2O$) in an 1 ml aliquot was measured by wet scintillation counting; the activity of $^3$H-$H_2O$ was measured after sparging the sample for >30 min with $N_2$ to remove excess $^3$H-$CH_4$, so that the net amount of $^3$H-$CH_4$ consumption can be estimated. The precision of the analysis was better than 5 %. Analyses of replicate samples yield values that differ by up to 30%.

MOx rates were calculated assuming first-order kinetics (Reeburgh et al., 1991; Valentine et al., 2001):

$$MOx = k'[CH_4] \quad (1)$$

where *k'* is the effective first-order rate constant calculated as the fraction of labeled methane oxidized per unit time, and [$CH_4$] is the in situ methane concentration. To verify first order kinetics we conducted time series incubations and measured the tracer consumption after 1, 2, 3, and 4 days. The MOx values were corrected for differences between in situ and incubation temperatures (Supplementary Material 1).

In addition, control samples were frequently taken and poisoned immediately after the addition of the tracer. The mean ($\bar{x}$) and standard deviation ($s$) of all controls sampled during a cruise were calculated and the limit of detection (LOD) was set as:

$$LOD = \bar{x} + 3s \quad (2)$$

The *LOD* was 0.02 nM day$^{-1}$ and 0.09 nM day$^{-1}$ for the summer 2013 and winter 2014 surveys, respectively.

2.2.3 Analysis of bacterial communities

The composition of the bacterioplankton assemblages was examined using denaturing gradient gel electrophoresis (DGGE) based on the 16S rRNA gene as described in Mau et al. (2013). In short, immediately after sampling, 8 L of water were filtered and the bacterial cells were concentrated on Nuclepore filters (0.2 µm pore size). The filters were stored on board at -20 °C and at -80 °C post cruise. DNA was extracted by an UltraClean Soil DNA Kit (MoBio Laboratories, USA). 16S rRNA gene specific PCR was conducted using the forward primer GM5 plus GC-clamp and the reverse primer 907RM (Muyzer et al., 1993) under conditions described by Gerdes et al. (2005). The PCR products (ca. 500 bp) were analyzed by DGGE according to the protocol of Muyzer et al. (1993). Clearly visible bands of the DGGE gels were excised from the gel. The DNA was reamplified by PCR (Gerdes et al., 2005) and sequenced. The 16S rRNA gene sequences were taxonomically assigned by SILVA Online Aligner (Pruesse et al., 2012).

The presence of methane-oxidizing bacteria was checked by searching for genes encoding the particulate methane monooxygenase (*pmoA*), a key enzyme of methanotrophs (McDonald et al., 2008). The *pmoA*-gene-specific PCR reaction was conducted by using the primer set “pmoA” and amplification conditions described in McDonald and Murrell (1997).

2.3 Methane concentration analysis by Under-Water Mass-Spectrometry (UWMS)

In addition to the conventional methane analysis, in situ methane concentrations were quantified with an UWMS during the summer 2013 cruise (Inspectr200-200, Bell et al., 2007; Gentz et al., 2013; Schlüter and Gentz, 2008; Short et al., 2001; Wenner et al., 2004). The fast sampling frequency (≤ 2 s) of the UWMS allows mapping of methane concentrations at much higher resolution than the commonly used CTD/rosette-sampling technique. The instrument consists of a membrane inlet system (MIS), an Inficon (Bad Ragaz, Switzerland) Transpector CPM 200 quadruple mass spectrometer, a Varian (Palo Alto, USA) turbo pump, a roughing pump, a peristaltic pump (KC

Denmark), an embedded PC, and a microcontroller. The UWMS was partly redesigned to include a cooling system (Ricor, K508), which lowers the detection limit for methane to 16 nM. The cooling system and the improvement of the detection limit are described in detail by Gentz and Schlüter (2012) and Schlüter and Gentz (2008). For reproducible gas permeation through the MIS, water is constantly heated to a steady temperature of 50°C and pumped at a flow rate of 3 ml $min^{-1}$ along the membrane by an external peristaltic pump.

The UWMS was deployed above the central gas seeps (cluster 1, Fig. 2) on 21.07.2013 (16:31 – 22:32 UTC) at five different water depths: just above the seafloor, 35 m, 28 m, 25 m, and 10 m. When the system had reached the respective depth, the research vessel moved slowly along a rectangular track (~125 m S-N, ~150 m E-W, Fig. 2C) surrounding the flares of cluster 1 and towed the UWMS, which continuously measured the methane concentrations. Each of the 5 tows (Fig. 2C) took approximately one hour and recorded 400-800 methane concentration values.

### 2.4 Estimation of methane fluxes

Advection, horizontal and vertical turbulent diffusion, sea-air flux, and microbial oxidation rates were quantified for the upper (0-30 m) and lower water column (30-40 m) during summer stratification (July 2013) and for the entirely mixed water column (0-40 m) in winter (January 2014).

The advective flux (*ADV*) was calculated by multiplying methane concentration (*C*) and current velocity (*v*):

$$ADV = vC \tag{3}$$

Methane concentrations were averaged above and below the thermocline from the summer survey, averages throughout the water column were calculated from the winter data. Current velocities refer to the resultant velocities calculated from the u and v component of the velocity vectors (Supplementary Material 2 and 3) and were averaged over the time period of sampling. The current data provided by the *Bundesamt für Seeschifffahrt und Hydrographie* (BSH) (www.bsh.de/de/Meeresdaten/Vorhersagen/Vorhersagemodelle/index.jsp) is based on wind and air temperature forecasts. Such modeled data has been validated by a few current measurements and has an uncertainty of ~10%. Therefore, the estimated advective flux has an uncertainty of ~15%.

If advective transport were to be uniform, then it would simply displace methane, but differences in current velocity and direction with depth lead to turbulent mixing, i.e., eddy diffusion (*DIF*). The

strength of small-scale motions that act to smooth out concentration gradients can be parameterized by the eddy diffusivity κ , such that mass transport is proportional to the mean concentration gradient (Largier, 2003; Roberts and Webster, 2002):

$$DIF = \kappa \left(\frac{\partial C}{\partial x}\right) \quad (4)$$

where κ is the horizontal or vertical diffusion coefficient in $m^2\ s^{-1}$. $\delta C/\delta x$ is the spatial concentration gradient in nM $m^{-1}$, estimated between the center and the outermost stations in the case of horizontal diffusion calculation, and the concentration gradient between the lower and upper water column in the case of vertical diffusion (Mau et al., 2012), calculated only for summer 2013.

$\kappa_y$, the horizontal diffusion coefficient, can range between 0.1 and 1000 $m^2\ s^{-1}$ (Largier, 2003; Sundermeyer and Price, 1998) depending on the proximity to land. $\kappa_y$ exponentially increases with distance from the shore: $\kappa_y$ is on the order of 1–10 $m^2\ s^{-1}$ if $y$~0.1 km, ~100 $m^2\ s^{-1}$ if $y$~10 km, and on the order of 1000 $m^2\ s^{-1}$ or greater if $y$~100–1000 km. As the study area is located more than 230 km from shore, we used a $\kappa_y$ of 1000 $m^2\ s^{-1}$ for our calculations. The vertical turbulent diffusion coefficient ($\kappa_z$) can vary between $10^{-3}$ and $10^{-6}$ $m^2\ s^{-1}$ depending on the energy in the water column (wind, tides, etc.) and stratification (Denman and Gargett, 1983; Wunsch and Ferrari, 2004). $\kappa_z$ was estimated according to the equation by Osborn (1980):

$$\kappa_z = \Gamma \frac{\epsilon}{N^2} \quad (5)$$

where Γ is the efficiency of mixing and assumed to be a constant of 0.2. We used published dissipation rates of turbulent kinetic energy (ϵ) in stratified shallow shelf seas (Palmer et al., 2008; Thorpe et al., 2008) and calculated the buoyancy frequency (N) from the available CTD-profiles. The results indicate that $\kappa_z$ is in the order of $10^{-4}$ to $10^{-6}$ $m^2\ s^{-1}$ during stratification. This rough approximation neglects hourly changes, which can vary by an order of magnitude. For example, Palmer et al. (2008) observed and calculated $\kappa_z$ to range between $10^{-4}$ and $10^{-5}$ $m^2\ s^{-1}$ over a tidal cycle. We used $10^{-4}$ $m^2\ s^{-1}$, which is a common cited value across the thermocline, in order to not underestimate the vertical eddy diffusion. These diffusion fluxes were estimated for all vertical profiles (all 10 CTD-stations). The uncertainty of these estimates is determined by that of the diffusion coefficient, which can vary by an order of magnitude.

The sea-air flux (*SAF*) was calculated as:

$$SAF = k_W(C_W - C_A) \quad (6)$$

where $k_W$ is the gas transfer velocity in cm $h^{-1}$, $C_W$ is the measured concentration of methane and $C_A$ is the methane concentration in atmospheric equilibrium, both in nM. We calculated $k_W$, which depends on wind speed and the temperature-dependent Schmidt number of the gas, using parameterization developed by McGillis et al. (2001). Mau et al. (2007) show that error associated with $k_W$ estimates can yield a flux uncertainty of 10-40 %. Wind speed was recorded 22 m above sea level onboard with a precision of 20% and corrected to the standard height of 10 m. $C_A$ was derived using the mean atmospheric methane concentration of Ocean Station M, Norway at 66°N and 2°E, in 2009 (1.874 ppm, http://www.esrl.noaa.gov/gmd/dv/data/), the Bunsen solubilities given by Wiesenburg and Guinasso (1979) and measured ocean temperature and salinities. The sea air flux was calculated for surface water samples of all 10 stations sampled in summer 2013 and winter 2014. As the sea air flux depends strongly on wind speed, the crucial uncertainties of this flux are associated with wind speed measurements and the parameterizations of the gas transfer velocity, which yield an overall uncertainty of less than an order of magnitude.

The oxidative loss (OL) was calculated by depth integration of the MOx rates:

$$OL = \overline{x}_{MOx} z \quad (7)$$

where $\overline{x}_{MOx}$ is the averaged MOx rate in nM $day^{-1}$ over the depth interval z in m. The depth interval is defined by the water stratification in the case of summer 2013 and covers the entire water depth in the case of winter 2014. Integration was done for all vertical profiles. The estimated oxidative loss of methane varies by <30% according to the precision of the oxidation rate measurement.

## 3 Results

### 3.1 Seep locations

Echosounder data collected during the winter survey indicate bubble emission in the area of the sampled transect (Fig. 2). The center station was located at a known gas bubble emission site or flare cluster, where several bubble streams occur in close proximity to each other. We observed an additional four flare clusters near the western sector of the transect, similar in seepage intensity as those from the central seep denoted as cluster 1 (Fig. 2A and C). In contrast, no additional flares were found in the area of the eastern sector. Although echosounder data point to bubbles rising to, or close to, the sea surface, no bubbles were visually identified at the sea surface due to rough sea

state. Seepage intensity showed no obvious variation related to tidal cycles, i.e., pressure variations due to high or low tides. The seeps were found to be active during all survey crossings. No echosounder data were collected in summer 2013, nonetheless, surfacing gas bubbles were visually documented when the sea was calm.

### 3.2 Oceanographic setting

In summer (July 2013) a seasonal thermocline separated surface (0-30 m) from bottom waters (30-42 m; Fig. 3). The surface water consisted of a 10-m thick mixed layer below which the temperature decreased stepwise from 17.5 to 7°C in 30 m. Lower salinity was observed at 15 and 25 m depths, which departed from the general value of 34.55. The stepwise decrease in temperature and the salinity variations indicate the successive development of several pycnoclines driven by increasing sea surface temperatures and steadily weakening wind activity in spring and summer. The oxygen concentrations increased from 220 µM at the surface to 240 µM at 30 m. In contrast to the surface water, the bottom water had a homogeneous temperature of 7.18 ± 0.09 °C, a salinity of 34.63 ± 0.02 and contained less oxygen (190 ± 5 µM).

In winter (January 2014) the entire water column was mixed (Fig. 3). The water had a temperature of 7°C, a salinity of 34.85, a density of 27.3 kg $m^{-3}$, and oxygen concentrations of 280 µM.

Modeled regional current data provided by the BSH indicate a dominant north-west transport throughout the water column with surface speed ranging between 0.06 and 0.27 m $s^{-1}$ (resultant speed). In summer, the eastern part of the transect was sampled when currents were directed to the north-west with an average speed of 0.24 m $s^{-1}$ and the western part was sampled when currents turned from north-west to south-west with an average speed of 0.19 m $s^{-1}$. In winter, the eastern part of the transect was sampled when water moved north-east turning north-west with an average speed of 0.22 m $s^{-1}$ and the western part was sampled when water also turned from north-east to north-west, but with an average speed of 0.1 m $s^{-1}$. Water speed and direction plots are given in Supplementary Material 2 and 3.

### 3.3 Methane concentrations

Consistent with the two layer structure observed on the hydrographic data, the methane concentration in summer 2013 also show a two layer distribution, with higher values in the bottom water (Fig. 4A, Supplementary Material 4). Methane concentrations in the surface water range from 4-518 nM with a median of 33 nM. Methane concentrations in the bottom water range between 40 and 1628 nM with a median of 391 nM. Highest concentrations in the surface water were found near

cluster 1 (170 nM) and generally decreased towards the outermost stations (to the west to 96 nM and to the east to 13 nM). Similarly, in the bottom water the highest methane concentrations were found at cluster 1 (600-700 nM), and concentrations decreased unevenly towards the outmost stations (200-300 nM). In both layers the methane concentrations exceeded the background concentration of ~20 nM as measured at a reference station located 32 km to the south-east of cluster 1 (Supplementary Material 5), and those reported by Grunwald et al. (2009) of 20 nM. Even this regional background value is supersaturated with respect to the atmospheric equilibrium concentration of 2.3-2.9 nM (at the relevant T/S conditions, Wiesenburg and Guinasso, 1979).

Much lower methane concentrations were found in winter 2014 (Fig. 4B, Supplementary Material 4). Highest values were observed only at one station near cluster 1 with concentrations reaching 656.6 nM. Such elevated values decreased rapidly horizontally (within 1 km) and were not encountered during repeated hydrocasts at the same location. The median of all methane concentration measurements along the transect was 22 nM, which is only slightly above the regional background concentration. In general, methane concentrations indicate a patchy spatial distribution as expected in an active seep area.

### 3.4 UWMS methane concentrations

The UWMS was deployed in the vicinity of flare cluster 1 in summer 2013 covering an area of 125 m by 150 m during instrument tow (Fig. 2C). Therefore, the hydrocast data (described in section 3.3) cover a much larger spatial scale (6 km) than sampled during the UWMS-tows. When the UWMS was towed close to bubble streams, it recorded methane concentrations that range over three orders of magnitude, from <16 nM (the detection limit, which is recorded as 0) to 2127 nM in surface waters (transects in 10 m, 25 m, 28 m). Values > 500 nM only were recorded during a period of ~11 min of the ~30 min tow at 25 m and ~4 min of the ~60 min tow at 28 m (Fig. 5). During bottom transects (30 m and 42 m) methane concentration are generally higher and range from 259 to 2213 nM. The median values of the records from the 10 m, 25 m, and 28 m water depth tows were <16 nM, 133 nM, and 158 nM, respectively, while the median in 30 m and 40 m depth were 508 and 679 nM.

UWMS and hydrocasts were deployed during different tidal phases to check the persistence of higher methane concentrations in the bottom water as tidal pressure changes can affect methane seepage (Boles et al., 2001). The UWMS tows were conducted during ebbing tides, when water levels fell from 0.18 to -0.27 m, whereas hydrocast samples were collected during rising tides, when sea level height increased from -0.21 to 0.06 m and from 0.04 to 0.16 m (Supplementary Material 6). The general pattern of lower concentrations in the surface and higher ones in the bottom water was

apparent at all stations, even though methane data were obtained using different techniques and samples were collected during different tidal phases.

### 3.5 Methane oxidation

Similar to the distribution of methane and co-located oceanographic data, the MOx rates calculated using equation (1) show a two layer pattern in summer 2013, but are uniform throughout the water column during the winter 2014 survey (Fig. 6A). In summer, MOx-rates in surface waters ranged between 0.04 and 9.2 nM $day^{-1}$ with a median of 0.1 nM $day^{-1}$ and in the bottom water between 1.6 and 840.9 nM $day^{-1}$ with a median of 4.0 nM $day^{-1}$. The total range of both layers (0.04- 840.9 nM $day^{-1}$) exceeds the range of MOx-rates observed during the winter survey (0.1-8.7 nM $day^{-1}$). The median of all MOx-rates measured in January 2014 was 0.2 nM $day^{-1}$.

### 3.6 Microbial communities

Molecular samples taken in summer 2013 show also a difference between surface and deep waters, whereas winter 2014 samples indicate a homogeneous spatial distribution of microorganisms (Fig. 7, Tab. 1). In summer 2013, different DGGE banding patterns reveal changes in microbial communities with depth. The surface water samples showed two strong bands (Fig. 7, bands 6, 7) that could be affiliated to the *Rhodobacteraceae* and two bands that could be assigned to the *Cyanobacteria / Synechococcus* clade (8, 9). The middle and bottom water samples were characterized by a strong chloroplast band (2), but also showed bands affiliated to the *Rhodobacteraceae* (5, 6). In the bottom water samples of the central station, we found an additional band, assigned to *Pseudoalteromonas* (10). The gel pattern of the winter samples showed no significant bands. The sequences of the faint bands excised were of low quality. Only two of the bands could be assigned to the *Rhodospirillaceae* (12, 13).

Neither the summer nor the winter bacterial communities exhibited known methanotrophic bacteria, even though the samples originate from an actively gas venting area. The absence of methanotrophic bacteria was further supported by the negative results of the *pmoA*-PCRs that targets a methanotroph molecular marker gene.

## 4 Discussion

The echosounder and visual observations at the central North Sea sites document gas emissions that in some cases reach the sea surface. This fraction of methane that is transported directly to the atmosphere by bubbles and released upon bursting might be significant, as was shown for example at the shallow seep field Coal Oil Point in California (<70 m). Here about half of the methane is

418 directly emitted to the atmosphere via bursting bubbles and the other half is injected in the water
419 (Clark et al., 2000), some fraction of which also escapes to the atmosphere. In this study, we focus on
420 the dissolved methane fraction that remains in the in the ocean and is available for microbial
421 oxidation.
422
423 4.1 Distribution of methane in summer and winter
424 Our highest dissolved methane concentrations, measured in the bottom water during the summer
425 survey, reach magnitudes similar to those observed at other shallow seep sites (Tab. 2). Our highest
426 value of 1627.7 nM is comparable to measurements downfield of the Coal Oil Point seep field (up to
427 1900 nM, Mau et al., 2012), although orders of magnitude less than measurements in the immediate
428 vicinity of the bubble plumes (Clark et al., 2003). Our highest value is higher than methane
429 concentrations reported for seep locations in the Tommeliten, North Sea (268 nM, Schneider von
430 Deimling et al., 2011), and offshore Svalbard, west of Prins Karls Forland (524 nM, Gentz et al., 2013).
431
432 Even though gas bubbles were observed at the sea surface during the summer survey, the dissolved
433 methane appears trapped beneath the seasonal thermocline (Fig. 4A). This observation is similar to
434 those at the Tommeliten site, where the dissolved methane plume was restricted beneath the
435 seasonal thermocline (Schneider von Deimling et al., 2011) although gas flares were imaged to rise
436 within 10 m of the sea surface. Elevated methane concentrations at other vent sites have also been
437 reported beneath a thermocline or halocline that hamper further ascent of dissolved methane to the
438 mixed layer. The dissolved methane plume originating from the 245 m deep seeps offshore Prins
439 Karls Forland was confined to water depths beneath a local halocline (Gentz et al., 2013). In the Baltic
440 Sea, summer stratification also leads to accumulation of methane below the thermocline (Gülzow et
441 al., 2013). At all these sites, an enhanced release of methane to the atmosphere is thought to occur
442 upon erosion of stratification. In contrast, the dissolved methane plume originating from seeps
443 situated between 5 and 70 m at the Coal Oil Point is dispersed within the mixed layer above the
444 thermocline (Mau et al., 2012), and as such it is not controlled by seasonal stratification patterns.
445
446 Trapping and accumulation of dissolved methane beneath a thermocline also is well documented in
447 lakes and freshwater reservoirs, where thermal stratification separates methane-poor, surface water
448 from the methane-rich, but anoxic, bottom water in e.g. a shallow floodplain lake in south-eastern
449 Australia (Ford et al., 2002), in a polyhumic lake in southern Finland (Kankaala et al., 2007), in the
450 subtropical Lake Kinneret in Israel (Eckert and Conrad, 2007), and in 8 freshwater reservoirs in India
451 (Narvenkar et al., 2013). In these locations, the accumulated methane is released to the atmosphere
452 at the onset of water column mixing in response to enhanced wind forcing and lower temperatures.

Our results show that in a seasonal stratified system, methane accumulation does not occur in winter, when the water column is well mixed (Fig. 4B). Methane concentrations were found to deviate only due to bubble ascent and were otherwise low and constant throughout the water. The median winter concentration of 22 nM is similar to the background values of 20 nM reported by Grunwald et al. (2009) for the German Bight, but is elevated relative to water originating from the Atlantic Ocean, which carries 2.5-3.5 nM of methane (Rehder et al., 1998) and to the methane background concentrations of <5 nM at Tommeliten (Niemann et al., 2005; Schneider von Deimling et al., 2011).

The observed difference between summer and winter dissolved methane concentrations also may be due to changes in seepage rate. The visual observation of gas bubbles during the summer, Schroot et al.'s (2005) sub-bottom profiler recording of gas plumes in the water column in August 2002, and our acoustic records of gas flares in the winter (Fig. 2B) indicate that seepage occurred during both seasons. Notwithstanding these observations, we recognize that we have insufficient temporal data coverage and that bubble release frequency, bubble size and initial methane content could vary between our surveys causing the difference in overall methane concentrations (Greinert and McGinnis, 2009; Leifer and Clark, 2001; McGinnis et al., 2006). However, even when a change in seepage regimes could affect the overall methane concentration, it would not explain the difference in the shape of the methane profiles observed between summer and winter surveys.

Discrete sampling bias and current variability also explains some fraction of the difference observed between summer and winter dissolved methane concentrations. The currents had a strong westward component during summer sampling with small north/south deviation throughout the water column (Supplementary Material 2), and thus the easternmost profiles are likely to be less influenced from direct bubble seepage (Fig. 4A). However, the profiles still show elevated methane concentration in the bottom water and lower concentrations in the shallow samples, consistent with methane trapping below the seasonal thermocline. We considered whether the low observed concentrations during winter may be due to the fact that during this survey we only partially sampled isolated plumes. Although the east-west-transect directly crust the cluster 1 flares (Fig. 2) and was oriented in direction of the tidal movement in that area, the stronger northward component of the current in winter (Supplementary Material 2 and 3) displaced methane plumes more rapidly than in summer. The elevated methane concentrations at the central seep site and along the western transect (although with much lower methane concentrations) suggest that we indeed sampled methane plumes (Fig. 4B). We note that the horizontal concentration gradient in surface water were 0.01 to

488 0.02 nM $m^{-1}$ during summer and winter, respectively. As a first order approximation we take the
489 highest concentration measured (39 in summer and 73 nM in winter) and a general current speed of
490 0.2 m $s^{-1}$ to estimate a plume size of ~4 km in diameter that would take ~5 h to cross our sampling
491 transect. Since we always sampled 5 stations in ~3 h for the eastern or western segments of the
492 transect, it seems rather unlikely that we completely missed a methane plume.
493
494 To summarize, even when methane concentrations may appear biased by discrete sampling, current
495 differences, and seepage rate, our data analyses suggest that the seasonal differences are real. Even
496 if the total magnitudes may be questioned, we are confident that the methane distribution pattern is
497 the result of seasonal stratification.
498
499 4.2 Interpreting methane oxidation rate data
500 Measured MOx-rates at our study site (Fig. 6A) lie at the upper end of MOx-rates previously reported
501 at sites elsewhere, which span over six orders of magnitude from 0.001-1000 nM $day^{-1}$ (Tab. 2,
502 Supplementary Material 7 by Mau et al., 2013). The rates measured in deep water samples during
503 summer (median 3.9 nM $day^{-1}$, up to 840 nM $day^{-1}$) equal those observed in the Gulf of Mexico after
504 the Deepwater Horizon event (median 10 nM $d^{-1}$, up to 820 nM $day^{-1}$) (Valentine et al., 2010). Even in
505 winter time, the estimated rates are high in comparison to those measured in the Eel River Basin, an
506 area of documented gas hydrate dissociation (Valentine et al., 2001) and match rates for the Coal Oil
507 Point seep field in the Santa Barbara Basin (Mau et al., 2012; Pack et al., 2011).
508
509 In spite of the reported high MOx values, our data reveal an overall low activity of methane oxidizing
510 microorganisms based on the values obtained for the rate constant *k'*, which provides an indication
511 of the relative activity in a water sample (Koschel, 1980). This is a first-order constant if the reaction
512 is solely dependent on the methane concentration and biomass does not increase during incubation.
513 Our experiments yielded similar *k'* values over a wide range of methane concentrations, from 4 to
514 728 nM (Fig. 6C). Furthermore, the good correlation between MOx-rates and methane concentration
515 (Fig. 6D) indicate that the biomass did not increase during incubation, thus validating our inferences
516 on microbial activity based on *k'* values. Based on 116 (out of 123) measurements we calculate an
517 average value for *k'* of 0.01 $day^{-1}$, i.e., a turnover time of 100 days (Fig. 6B). This value matches the
518 value *k'* derived from our time series incubation results (0.01 $day^{-1}$, n=4), which show that only 5-6%
519 of the added $^{3}$H-methane tracer was consumed by microbial activity after 4 incubation days
520 (Supplementary Material 8). The time series show a linear increase of tracer oxidation and the
521 function derived from Fig. 6D that yield a first-order relationship between methane oxidation rates
522 and methane concentration with *k'*=0.01. If we use the average *k'* and methane concentrations that

span 4-728 nM, the resulting oxidation rates (Eq. 1) range between 0.04-7.3 nM $day^{-1}$. Thus relatively high MOx-rates here reflect primarily high methane concentrations, and must not be taken as indication of a high microbial turnover.

We note that 7 data points collected in summer near flare cluster 1 (stations 12 and 13) had *k'* values ranging from 0.08 to 0.64 $day^{-1}$, significantly higher than the rest of the measurements. These high values multiplied with high corresponding methane concentrations gave the highest MOx-values measured during this study. These elevated *k'* values may indicate an increase in biomass and/or an increase in activity of the methane oxidizing community in the water sample during incubation.

The general low activity of methane oxidizing microorganisms is further supported by molecular analysis of filtered matter from seawater. Consistently, DGGE and *pmoA* analysis did not reveal the presence of any known methanotrophic bacteria or *pmoA*-genes. Either methanotrophs were only present in low numbers and/or poorly matched to the used PCR primers and, thus, were not detected (Hansman, 2008). We also note that although no canonical methanotrophs were detectable in shallow marine waters (< 200 m) in the Pacific, Atlantic, and the Gulf of Mexico, further analyses of these samples revealed sequences closely related to those coding for methane monooxygenase (Elsaied et al., 2004; Tavormina et al., 2008; Tavormina et al., 2013; Valentine, 2011; Wasmund et al., 2009), an enzymatic hallmark of aerobic methanotrophs. We recognize that not having detected methanotrophs in our samples does not preclude their presence in the water column.

Even though during summer stratification methane is trapped beneath the seasonal thermocline, the resulting higher methane concentrations do not appear to enhance the activity of methane oxidation microbes. The residence time of central North Sea water is about 1.5-2 years (Prandle, 1984; Ursin and Andersen, 1978) and thermal stratification prevails for 4 months, which may provide sufficient time to establish a methanotrophic community. However, microbial turnover times in bottom water samples are consistently low and we were not able to identify methanotrophic organisms in the water column. Doubling times of planktonic marine methanotrophs are not known to the authors, but if we assume a doubling time of ~10 h as known from cultured methanotrophs (Baani and Liesack, 2008; Khadem et al., 2010) or a doubling time of 3.5 days estimated after the Deep Water Horizon incident in the Gulf of Mexico (Kessler et al. (2011), a methanotrophic community could potentially develop in the central North Sea during the 4 months where stratification leads to enhanced methane content in the bottom water. Even if the doubling time of methanotrophs in the field was longer than in culture as nutrients and substrates can be limiting, the residence time of the water would permit growth. Possible limitations may be a lack of essential trace elements or that the

methane oxidizing microorganisms are facultative methanotrophs (Tavormina et al., 2013), i.e., not necessarily depending on methane.

In summary, even though total MOx rates are necessary to constrain overall methane budgets and carbon cycles, to better characterize microbial activity among different ecosystems it is necessary to also report data on the microbial turnover rates at each site. The low turnover rates measured here are consistent with molecular analyses that failed to identify methanotrophic bacteria or *pmoA*-genes. Enhanced methane concentrations do not appear to foster higher turnover rates.

### 4.3 Methane transport in the North Sea is faster than oxidation

When methane enters the water column, either directly from the seep or by dissolution/gas exchange from ascending bubbles, it is transported by ocean currents and spreads by horizontal and vertical eddy diffusion. Methane oxidizing microorganisms can consume dissolved methane in the water column, and methane will be transferred into the atmosphere if its concentration in the mixed layer is higher than saturation.

As a first order evaluation of the relative importance of these transport and loss processes, we estimated the advective transport, the horizontal and vertical eddy diffusion, sea-air flux, and integrated the MOx-rates (see methods and Mau et al., 2012). Summer fluxes for the bottom (30-43m) and surface waters (0-30 m), were estimated using data collected in July 2013, and winter fluxes were derived for the entire unstratified water column (0-42m) using data from January 2014. All fluxes were estimated in units of nmol $m^{-2}$ $s^{-1}$. These flux estimates may vary by up to one order of magnitude due to precision of the measurements, the parameterization of the gas transfer velocity, and assumed diffusion coefficients (see method section for more detail).

The results shown in Fig. 8 revealed that in both summer and winter seasons, horizontal advection and eddy diffusion are the dominant processes transporting and diluting the emitted methane. The loss processes, i.e., sea air flux and microbial oxidation, are more than 4-orders of magnitude lower than physical horizontal transport processes.

Vertical mixing due to internal waves resulting from proximity to the elevation of the Dogger Bank cannot be ruled out. Estimates of $\kappa_z$ for the shelf break range in the order of $0.5\text{-}0.7 \cdot 10^{-4}$ $m^2$ $s^{-1}$ (Palmer et al., 2008). Our vertical fluxes based on $\kappa_z = 10^{-4}$ $m^2$ $s^{-1}$, thus include the enhanced mixing by internal waves that support increased transport across the seasonal thermocline.

Not surprisingly, the sea-air flux removes more methane from the water column during winter due to increased wind speed and storm sparging (Shakhova et al., 2013). More unexpectedly, our flux estimates revealed that within our study area the amount of methane that is transported in summer via vertical diffusion into the surface water is of similar magnitude than the loss by oxidation in the bottom water, even water stratification leads to enhanced methane concentrations at depth. When lower wind speeds prevail, methane oxidation was estimated to be of similar magnitude as the gas transfer to the atmosphere. However, our estimates do not include potential transport to the atmosphere as bottom water reach topographic highs such as the Dogger Bank or areas with no stratification.

Our findings are similar to those reported by Scranton and McShane (1991) for the Southern Bight of the North Sea. They found methane oxidation (0.00023-0.3 nM $day^{-1}$) and methane loss to the atmosphere (0.00026-7.5 nM $day^{-1}$) of a similar magnitude, but the latter increased during periods of high wind speed. Estimates for the shallow Coal Oil Point methane plume in the Santa Barbara Basin (Mau et al., 2012) show that at this location 0.05 mol $day^{-1}$ are oxidized in the surface water and 0.03 mol $day^{-1}$ are transferred to the atmosphere, i.e., both methane loss processes are of similar magnitude.

## 5 Conclusions

1. Observations at a shallow gas seep site in the central North Sea document elevated methane concentrations below the thermocline during summer stratification. In contrast, regional background methane concentrations were observed throughout the water column in the winter, when the water column is well mixed.
2. At our study site, physical transport processes always outcompete microbial methane oxidation. Horizontal advection and diffusion of methane are consistently higher than vertical transport, even within order of magnitude uncertainties. During periods of high wind speed (fall and winter), more methane reaches the atmosphere than is oxidized in the water; in summer the loss to the atmosphere and the oxidation terms are of similar magnitude.
3. We show that MOx rates alone cannot be used to characterize the ecosystem microbial activity, as these values are scaled to the methane concentration. We instead propose to include interpretation of *k'* values as an indicator of microbial activity. Averaged *k'* values generate a more realistic parameter than values based solely on replicate samples as further documented by our work-intensive time series incubations.
4. Our results demonstrate that trapping of methane below a seasonal thermocline does not necessarily lead to enhance microbial oxidation. Further research is needed to elucidate why

stratification over a summer season of 4 months does not enhance methanotrophy enough to significantly hamper methane release to the atmosphere upon water column mixing.

Author contribution

S. M. designed study, measured methane concentrations and methane oxidation rates, calculated the fluxes, wrote the manuscript

T.G., R. M., and M.S. deployed the UWMS and post-processed the data

J.-H. K., M. R., H. S., and P. W. collected and post-processed hydroacoustic data

M. T. interpreted methane oxidation rate data, edited manuscript

E. H. implemented and interpreted molecular analyses

Acknowledgement

We are indebted to the captain, crew, and scientific research party of the research vessel *Heincke* (cruise HE406 and HE413), especially to the applicants of RV Heincke cruises HE 406 and HE413 and organizers Sabine Kasten and Gerhard Bohrmann. We like to thank Sven Klüber, Eva Kirschenmann, and Monika Wiebe for their help collecting and analyzing samples on board and in the laboratory. We are grateful to Tessa Clemes from Alfred Wegener Institute Helmholtz Centre for Polar and Marine Research (Bremerhaven, Germany), who implemented the microbial analyses. We like to thank Antje Boetius, Gunter Wegener, and Mirja Meiners from the Max Planck Institute for Marine Microbiology (Bremen, Germany) for providing scientific equipment and laboratory support for oxidation rate measurements. Marta Torres acknowledges support through a fellowship from the Hanse Wissenschaftskolleg. This work is part of the DFG project 'Limitations of Marine Methane Oxidation' (MA 3961/2-1).

References

Baani, M. and Liesack, W.: Two isozymes of particlate methane monooxygenase with different methane oxidation kinetics are found in Methylocystis sp. strain SC2, PNAS, 105, 10203-10208, 2008.

Bange, H. W.: Nitrous oxide and methane in European coastal waters, Estuar. Coast. Shelf S., 70, 361-374, 2006.

Bange, H. W., Bartell, U. H., Rapsomanikis, S., and Andreae, M. O.: Methane in the Baltic and North Seas and a reassessment of the marine emissions of methane, Global Biogeochem. Cy., 8, 465-480, 1994.

Bell, R. J., Short, R. T., Van Amerom, F. H. W., and Byrne, R. H.: Calibration of an in situ membrane inlet mass spectrometer for measurements of dissolved gases and volatile organics in seawater, Environ. Sci. Technol., 41, 2007.

Berner, R. A.: Biogeochemical cycles of carbon and sulfur and their effect on atmospheric oxygen over Phanerozoic time, Palaeogeogr. Palaeocl., 73, 97-122, 1989.

Boetius, A., Ravenschlag, K., Schubert, C. J., Rickert, D., Widdel, F., Gieskes, A., Amann, R., Jørgensen, B. B., Witte, U., and Pfannkuche, O.: A marine microbial consortium apparently mediating anaerobic oxidation of methane, Nature, 407, 623-626, 2000.

Boles, J. R., Clark, J. F., Leifer, I., and Washburn, L.: Temporal variation in natural methane seep rate due to tides, Coal Oil Point area, California, J. Geophys. Res., 106, 27077-27086, 2001.

Cicerone, R. J. and Oremland, R. S.: Biochemical aspects of atmospheric methane, Global Biogeochem. Cy., 2, 299-327, 1988.

Clark, J. F., Leifer, I., Washburn, L., and Luyendyk, B. P.: Compositional changes in natural gas bubble plumes: observations from the Coal Oil Point marine hydrocarbon seep field, Geo-Mar. Lett., 23, 187-193, 2003.

Denman, K. L. and Gargett, A. E.: Time and space scales of vertical mixing and advection of phytoplankton in the upper ocean, Limnol. Oceanogr., 28, 801-815, 1983.

Eckert, W. and Conrad, R.: Sulfide and methane evolution in the hypolimnion of a subtropical lake: a three-year study, Biogeochemistry, 82, 67-76, 2007.

Elsaied, H. E., Hayashi, T., and Naganuma, T.: Molecular analysis of deep-sea hydrothermal vent aerobic methanotrophs by targeting genes of 16S rRNA and particulatemethane monooxygenase, Mar. Biotechnol., 6, 503–509, 2004.

Etiope, G., Lassey, K. R., Klusman, R. W., and Boschi, E.: Reappraisal of the fossil methane budget and related emission from geologic sources, Geophys. Res. Lett., 35, L09307, 2008.

Ford, P. W., Boon, P. I., and Lee, K.: Methane and oxygen dynamics in a shallow floodplain lake: the significance of period stratification, Hydrobiologia, 485, 97-110, 2002.

767 Gentz, T., Damm, E., Schneider von Deimling, J., Mau, S., McGinnis, D. F., and Schlüter, M.: A water
768 column study of methane around gas flares located at the West Spitsbergen continental margin,
769 Cont. Shelf Res., doi: 10.1016/j.csr.2013.07.013, 2013. 2013.
770 Gentz, T. and Schlüter, M.: Underwater cryotrap-membrane inlet system (CT-MIS) for improved in
771 situ analysis of gases, Limnol. Oceanogr.: Methods, 10, 317-328, 2012.
772 Gerdes, B., Brinkmeyer, R., Dieckmann, G., and Helmke, E.: Influence of crude oil on changes of
773 bacterial communities in Arctic sea-ice, FEMS Microbiol. Ecol., 53, 129-139, 2005.
774 Greinert, J. and McGinnis, D. F.: Single bubble dissolution model - The graphical user interface SiBu-
775 GUI, Environ. Model. Softw., 24, 1012-1013, 2009.
776 Grunwald, M., Dellwig, O., Beck, M., Dippner, J. W., Freund, J. A., Kohlmeier, C., Schnetger, B., and
777 Brumsack, H.-J.: Methane in the southern North Sea: Sources, spatial distribution and budgets,
778 Estuar. Coast. Shelf S., 81, 445-456, 2009.
779 Gülzow, W., Rehder, G., Schneider v. Deimling, J., Seifert, T., and Tóth, Z.: One year of continuous
780 measurements constraining methane emissions from the Baltic Sea to the atmosphere using a ship of
781 opportunity, Biogeosciences, 10, 81-99, 2013.
782 Holt, J. and Umlauf, L.: Modelling the tidal mixing fronts and seasonal stratification of the Northwest
783 European Continental shelf, Cont. Shelf Res., 28, 887-903, 2008.
784 Howarth, M. J.: North Sea Circulation. In: Encyclopedia of Ocean Sciences, Steele, J. H. (Ed.),
785 Academic Press, Oxford, 2001.
786 IPCC: Climate Change 2013 – The Physical Science Basis – Contribution of Working Group I to the
787 Fifth Assessment Report of the Intergovernmental Panel on Climate Change, Cambridge University
788 Press, Cambridge, 2013.
789 Jørgensen, B. B. and Kasten, S.: Sulfur Cycling and Methane Oxidation. In: Marine Geochemistry,
790 Schulz, H. D. and Zabel, M. (Eds.), Springer, Berlin Heidelberg 2006.
791 Kankaala, P., Taipale, S., Nykänen, H., and Jones, R. I.: Oxidation, efflux, and isotopic fractionation of
792 methane during autumnal turnover in a polyhumic, boreal lake, J. Geophys. Res., 112, G02003, 2007.
793 Kessler, J. D., Valentine, D. L., Redmond, M. C., Du, M., Chan, E. C., Mendes, S. D., Quiroz, E. W.,
794 Villanueva, C. J., Shusta, S. S., Werra, L. M., Yvon-Lewis, S. A., and Weber, T. C.: A persistent oxygen
795 anomaly reveals the fate of spilled methane in the deep Gulf of Mexico, Science, 331, 312-315, 2011.
796 Khadem, A. F., Pol, A., Jetten, M. S. M., and Op den Camp, H. J. M.: Nitrogen fixation by the
797 verrucomicrobial methanotroph '*Methylacidiphilum fumariolicum*' SolV, Microbiology, 156, 1052-
798 1059, 2010.
799 Killops, S. D. and Killops, V. J.: An Introduction to Organic Geochemistry, Longman, Essex, United
800 Kingdom, 1993.

King, G. M.: Ecological aspects of methane oxidation, a key determinant of global methane dynamics, Adv. Microb. Ecol., 12, 432-468, 1992.

Koschel, R.: Untersuchungen zur Phosphataffinitat des Planktons in der euphotischen Zone von Seen, Limnologica, 12, 141-145, 1980.

Kröncke, I. and Knust, R.: The Dogger Bank: a special ecological region in the central North Sea, Helgoländer Meeresunters., 49, 335-353, 1995.

Largier, J. L.: Considerations in estimating larval dispersal distances from oceanographic data, Ecol. Appl., 13, 71-89, 2003.

Leifer, I. and Clark, J.: Modeling trace gases in hydrocarbon seep bubbles. Application to marine hydrocarbon seeps in the Santa Barbara Channel, Russ. Geol. Geophys., 43, 613-621, 2001.

Magen, C., Lapham, L. L., Pohlman, J. W., Marshall, K., Bosman, S., Casso, M., and Chanton, J. P.: A simple headspace equilibration method for measuring dissolved methane, Limnol. Oceanogr. Meth., 12, 637–650, 2014.

Mau, S., Blees, J., Helmke, E., Niemann, H., and Damm, E.: Vertical distribution of methane oxidation and methanotrophic response to elevated methane concentrations in stratified waters of the Arctic fjord Storfjorden (Svalbard, Norway), Biogeosciences, 10, 6267–6278, 2013.

Mau, S., Heintz, M. B., and Valentine, D. L.: Quantification of $CH_4$ loss and transport in dissolved plumes of the Santa Barbara Channel, California, Cont. Shelf Res., 32, 110-120, 2012.

Mau, S., Valentine, D. L., Clark, J. F., Reed, J., Camilli, R., and Washburn, L.: Dissolved methane distributions and air-sea flux in the plume of a massive seep field, Coal Oil Point, California, Geophys. Res. Lett., 34, L22603, 2007.

McDonald, I. R., Bodrossy, L., Chen, Y., and Murrell, J. C.: Molecular ecology techniques for the study of aerobic methanotrophs, Appl. Environ. Microb., 74, 1305-1315, 2008.

McDonald, I. R. and Murrell, J. C.: The particulate methane monooxygenase gene pmoA and its use as a functional gene probe for methanotrophs, FEMS Microbiol. Lett., 156, 205-210, 1997.

McGillis, W., R., Edson, J., B., Ware, J., D., Dacey, J., W. H., Hare, J., E., Fairall, C., W., and Wanninkhof, R.: Carbon dioxide flux techniques performed during GasEx-98, Mar. Chem., 75, 267-280, 2001.

McGinnis, D. F., Greinert, J., Artemov, Y., Beaubien, S. E., and Wuest, A.: Fate of rising methane bubbles in stratified waters: How much methane reaches the atmosphere?, J. Geophys. Res., 111, 15, 2006.

Muyzer, G., de Waal, E., and Uitterlinden, A.: Profiling of complex microbial populations by denaturing gradient gel electrophoresis analysis of polymerase chain reaction-amplified genes coding for 16S rRNA, Appl. Environ. Microbiol., 59, 695-700, 1993.

834 Narvenkar, G., Naqvi, S. W. A., Kurian, S., Shenoy, D. M., Pratihary, A. K., Naik, H., Patil, S., Sarkar, A.,
835 and Gauns, M.: Dissolved methane in Indian freshwater reservoirs, Environ. Monit. Assess., 185,
836 6989–6999, 2013.
837 Niemann, H., Elvert, M., Hovland, M., Orcutt, B., Judd, A. G., Suck, I., Gutt, J., Joye, S., Damm, E.,
838 Finster, K., and Boetius, A.: Methane emission and consumption at a North Sea gas seep (Tommeliten
839 area), Biogeosciences 2, 335-351, 2005.
840 Niewöhner, C., Hensen, C., Kasten, S., Zabel, M., and Schulz, H. D.: Deep sulfate reduction completely
841 mediated by anaerobic methane oxidation in sediments of the upwelling area off Namibia, Geochim.
842 Cosmochim. Ac., 62, 455-464, 1998.
843 Osborn, T. R.: Estimates of the local rate of diffusion from dissipation measurements, J. Phys.
844 Oceanogr., 10, 83-89, 1980.
845 Otto, L., Zimmermann, J. T. F., Furnes, G. K., Mork, M., Saetre, R., and Becker, G.: Review of the
846 physical oceanography of the North Sea, Neth. J. Sea Res., 26, 161-238, 1990.
847 Pack, M. A., Heintz, M. B., Reeburgh, W. S., Trumbore, S. E., Valentine, D. L., Xu, X., and Druffel, E. R.
848 M.: A method for measuring methane oxidation rates using low-levels of $^{14}$C-labeled methane and
849 accelerator mass spectrometry, Limnol. Oceanogr.: Methods, 9, 245-260, 2011.
850 Palmer, M. R., Rippeth, T. P., and Simpson, J. H.: An investigation of internal mixing in a seasonally
851 stratified shelf sea, J. Geophys. Res., 113, 2008.
852 Pingree, R. D. and Griffiths, D. K.: Tidal Fronts on the Shelf Seas Around the British Isles, J. Geophys.
853 Res., 83, 4615-4622, 1978.
854 Prandle, D.: A modelling study of the mixing of $^{137}$Cs in the seas of the European continental shelf,
855 Philos. T. Roy. Soc. A 310, 407-436, 1984.
856 Pruesse, E., Peplies, J., and Glöckner, F. O.: SINA: accurate high-throughput multiple sequence
857 alignment of ribosomal RNA genes, Bioinformatics, 28, 1823-1829, 2012.
858 Reeburgh, W. S., Ward, B. B., Whalen, S. C., Sandbeck, K. A., Kilpatrick, K. A., and Kerkhof, L. J.: Black
859 Sea methane geochemistry, Deep-Sea Res., 38, S1189-S1210, 1991.
860 Rehder, G., Keir, R. S., Suess, E., and Pohlmann, T.: The multiple sources and patterns of methane in
861 North Sea waters, Aquat. Geochem., 4, 403-427, 1998.
862 Roberts, P. J. W. and Webster, D. R.: Turbulent Diffusion. In: Environmental Fluid Mechanics-Theories
863 and Application, Shen, H., Cheng, A., Wang, K.-H., Teng, M. H., and Liu, C. (Eds.), Amer. Soc. Civil Eng.
864 Press, Reston, Virginia, 2002.
865 Schlüter, M. and Gentz, T.: Application of membrane inlet mas spectrometry for online and in situ
866 analysis of methane in aquatic environments, J. Am. Soc. Mass Spectrom., 19, 1395-1402, 2008.

867 Schneider von Deimling, J., Rehder, G., Greinert, J., McGinnis, D. F., Boetius, A., and Linke, P.:
868 Quantification of seep-related methane gas emissions at Tommeliten, North Sea, Cont. Shelf Res., 31,
869 876-878, 2011.
870 Schroot, B. M., Klaver, G. T., and Schuettenhelm, T. E.: Surface and subsurface expressions of gas
871 seepage to the seabed - examples from the southern North Sea, Mar. Petrol. Geol., 22, 499-515,
872 2005.
873 Scranton, M. I. and McShane, K.: Methane fluxes in the southern North Sea: The role of European
874 rivers, Cont. Shelf Res., 11, 37-52, 1991.
875 Shakhova, N., Semiletov, I., Leifer, I., Sergienko, V., Salyuk, A., Kosmach, D., Chernykh, D., Stubbs, C.,
876 Nicolsky, D., Tumskoy, V., and Gustafsson, Ö.: Ebullition and storm-induced methane release from
877 the East Siberian Arctic Shelf, Nature Geoscience, 7, 64-70, 2013.
878 Short, R. T., Fries, D. P., Kerr , M. L., Lembke, C. E., Toler, S. K., Wenner, P. G., and Byrne, R. H.:
879 Underwater mass spectrometers for in situ chemical analysis of the hydrosphere, J. Am. Soc. Mass
880 Spectrom., 12, 676-682, 2001.
881 Sundermeyer, M. A. and Price, J. F.: Lateral mixing and the North Atlantic tracer release experiment:
882 observations and numerical simulations of Lagrangian particles and a passive tracer, J. Geophys. Res.,
883 103, 21481-21497, 1998.
884 Sündermann, J. and Pohlmann, T.: A brief analysis of North Sea physics, Oceanologia, 53, 663-689,
885 2011.
886 Tavormina, P. L., Ussler III, W., and Orphan, V. J.: Planktonic and sediment-associated aerobic
887 methanotrophs in two seep systems along the North American Margin, Appl. Environ. Microbiol., 74,
888 3985-3995, 2008.
889 Tavormina, P. L., Ussler, W., Steele, J. A., Connon, S. A., Klotz, M. G., and Orphan, V. J.: Abundance
890 and distribution of diverse membrane-bound monooxygenase (Cu-MMO) genes within the Costa Rica
891 oxygen minimum zone, Environ. Microbiol. Reports, 5, 414-423, 2013.
892 Thorpe, S. A., Green, J. A. M., Simpson, J. H., Osborn, T. R., and Nimmo Smith, W. A. M.: Boils and
893 turbulences in a weakly stratified shallow tidal sea, J. Phys. Oceanogr., 38, 1711-1730, 2008.
894 Ursin, E. and Andersen, K. P.: A model of the biological effects of eutrophication in the North Sea,
895 Rapp. P.-v. Reun. Cons. Int. Explor. Mer, 172, 366-377, 1978.
896 Valentine, D. L.: Emerging topics in marine methane biogeochemistry, Annu. Rev. Mar. Sci., 3, 147-
897 171, 2011.
898 Valentine, D. L., Blanton, D. C., Reeburgh, W. S., and Kastner, M.: Water column methane oxidation
899 adjacent to an area of active hydrate dissociation, Eel River Basin, Geochim. Cosmochim. Ac., 65,
900 2633-2640, 2001.

Valentine, D. L., Kessler, J. D., Redmond, M. C., Mendes, S. D., Heintz, M. B., Farwell, C., Hu, L., Kinnaman, F. S., Yvon-Lewis, S., Du, M., Chan, E. W., Tigreros, F. G., and Villanueva, C. J.: Propane respiration jump-starts microbial response to a deep oil spill, Science, 330, 208-211, 2010.

Wasmund, K., Kurtboke, D. I., Burns, K. A., and Bourne, D. G.: Microbial diversity in sediments associated with a shallow methane seep in the tropical Timor Sea of Australia reveals a novel aerobic methanotroph diversity, FEMS Microbiol. Ecol., 68, 142–151, 2009.

Wenner, P. G., Bell, P. G., van Amerom, F. H. W., Toler, S. K., Edkins, J. E., Hall, M. L., Koehn, K., Short, R. T., and Byrne, R. H.: Environmental chemical mapping using an underwater mass spectrometer, Trac-Trend Anal. Chem., 23, 288-295, 2004.

Wiesenburg, D. A. and Guinasso, J. N. L.: Equilibrium solubilities of methane, carbon monoxide, and hydrogen in water and sea water, J. Chem. Eng. Data, 24, 356-360, 1979.

Wunsch, C. and Ferrari, R.: Vertical mixing, energy, and the general circulation of the oceans, Annu. Rev. Fluid Mech., 36, 281-314, 2004.

935 Tables

936 Tab. 1 Classification of partial 16S rRNA gene sequences (Fig. 7) to bacterial taxa performed with the
937 Silva classifier (Pruesse et al., 2012). The confidence value (0–1) for assignment at the level of class
938 and genus is given in parentheses.

| No. | Class | Family |
|---|---|---|
| 1 | Alphaproteobacteria (0.4) | *SAR11 clade* (0.2) |
| 2 | Cyanobacteria (1) | *Chloroplast* (1) |
| 3 | Alphaproteobacteria (1) | *Rhodobacteraceae* (1) |
| 4 | Bacteroidetes incertae sedis (0.43) | *Marinifilum* (0.4) |
| 5 | Alphaproteobacteria (1) | *Rhodobacteraceae* (1) |
| 6 | Alphaproteobacteria (1) | *Rhodobacteraceae* (1) |
| 7 | Alphaproteobacteria (1) | *Rhodobacteraceae* (1) |
| 8 | Cyanobacteria (1) | *Synechococcus* (1) |
| 9 | Cyanobacteria (1) | *Synechococcus* (1) |
| 10 | Gammaproteobacteria (1) | *Pseudoalteromonadaceae* (1) |
| 11 | Proteobacteria (0.36) | |
| 12 | Alphaproteobacteria (1) | *Rhodospirillaceae* (0.8) |
| 13 | Alphaproteobacteria (0.91) | *Rhodospirillaceae* (0.7) |

939
940
941
942
943
944
945
946
947
948
949
950
951
952
953
954
955

956 Tab. 2 Comparison of highest methane concentrations, methane oxidation rates, and sea-air fluxes from different locations

| **Location** | **Methane concentration** | **MOx-rate** | **SAF** | **Reference** |
|---|---|---|---|---|
| | *up to nM* | *nM day$^{-1}$* | *nmol m$^{-2}$ s$^{-1}$* | |
| ***Seep sites*** | | | | |
| central North Sea | 1628 | 0.04-840 | 0.02-8.3 | this study |
| Coal Oil Point, Santa Barbara Basin | 1900 | 0.02-30 | 1.8 | Mau et al., 2012; Pack et al., 2011 |
| Tommeliten, North Sea | 268 | | 10.8* | Schneider von Deimling et al., 2011 |
| west of Prins Karls Forland, Svalbard | 524 | up to 0.8 | | Gentz et al., 2013 |
| Eel River Basin | 300 | 0.002-0.8 | | Valentine et al., 2001 |
| ***Deepwater Horizon event*** | | | | |
| Gulf of Mexico | 180000 | up to 820 | | Valentine et al., 2010 |
| Gulf of Mexico | 1000000 | up to 5900 | | Crespo-Medina et al., 2014 |
| ***Overall areas*** | | | | |
| Baltic Sea | 38 | | 0.008-0.2 | Gülzow et al., 2013 |
| Southern Bight of the North Sea | 372 | 0.0002-0.3 | 0.07-7 | Scranton and McShane (1991) |
| general European shelf estimate | 21 | | 0.11-0.24 | Bange, 2006 |
| ***Lakes*** | | | | |
| floodplain lake in south-eastern Australia | 50000 | | 8.3-2700 | Ford et al., 2002 |
| polyhumic lake in southern Finland | 150000 | 30-14400 | 0.5-695 | Kankaala et al., 2007 |
| the subtropical Lake Kinneret in Israel | 450000 | | | Eckert and Conrad, 2007 |
| freshwater reservoirs in India | 156000 | | | Narvenkar et al., 2013 |

*direct transport via bubbles

957

958

959 Figures

960 Fig. 1: Location of the study area in the central North Sea. The main currents are shown following
961 Howarth (2001). The map was drawn using GeoMapApp with 40 m contours.

962

963 Fig. 2: A) Overview of gas flares mapped in January 2014 and CTD stations sampled in July 2013 (S12-
964 S21) and January 2014 (W2-W12). Flares cluster in 5 distinct areas (cluster 1-5) and reach to 6 m
965 from the sea surface (e.g. cluster 2 (B)), which corresponds to the echosounder's transducer depth.
966 Hence, most likely the gas transport extends to the sea surface. Cluster 1 corresponds to the gas seep
967 area investigated by Gentz (2013) (C).

968

969 Fig. 3: Depth profiles of potential temperature, salinity, density (sigma theta), and oxygen for all
970 stations in both summer and winter field programs.

971

972 Fig. 4: A-B Contour plots of the dissolved methane concentrations measured in the water column in
973 July 2013 and January 2014. The 6 km transect was divided into an eastern (positive numbers) and
974 western part (negative numbers) starting from the center station at 0 km. Note the different
975 methane concentration scales, which are necessary to properly display the different concentration
976 ranges. The black dots indicate the sampled water depths.

977

978 Fig. 5: Methane concentrations recorded by UWMS on 21.07.2013 in the vicinity of flare cluster 1
979 (Fig. 2C) at different water depth. The detection limit of the instrument is 16 nM, all measurements
980 below this value are recorded as 0. Apart from temporal and spatial elevations most likely due to
981 bubble streams, the background value is elevated throughout the recording time in 30 and 42 m
982 water depth.

983

984 Fig. 6: Methane oxidation rates versus water depth measured with $^{3}$H-methane in July 2013 and in
985 January 2014 (A). B The first order rate constant *k'* of summer and winter samples indicating the
986 relative activity of the water. C *k'* versus methane concentration illustrate similar *k'* values over a
987 wide range of methane concentration. D Methane oxidation rates versus methane concentrations
988 shows for most of the data a first order function: $MOx=0.01[CH_4]^1$ (function with $R^2$ of 0.92 derived
989 from winter data and with $R^2$ of 0.85 from summer data).

990

991 Fig. 7: DGGE profile of 16S rRNA gene fragments of samples from different depth and stations in the
992 central North Sea. Numbers on the lines indicate excised and successfully sequenced DGGE bands,
993 whose phylogenetic assignment is listed in Tab. 1.

994

995 Fig. 8: Sketch of transport and loss terms estimated for the study area in nmol $m^{-2}$ $s^{-1}$.

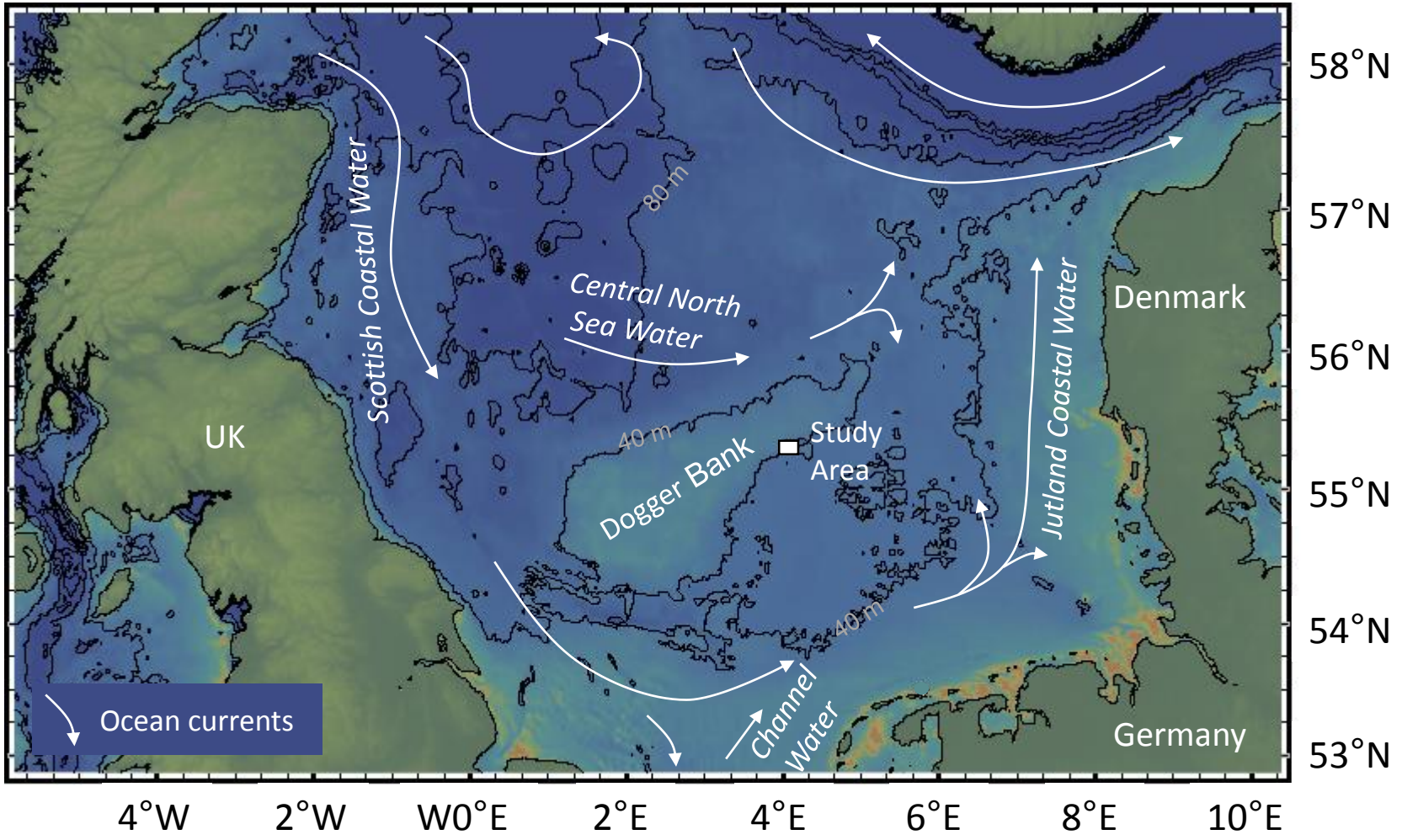


Fig. 1: Location of the study area in the central North Sea. The main currents are shown following Howarth (2001). The map was drawn using GeoMapApp with 40 m contours.

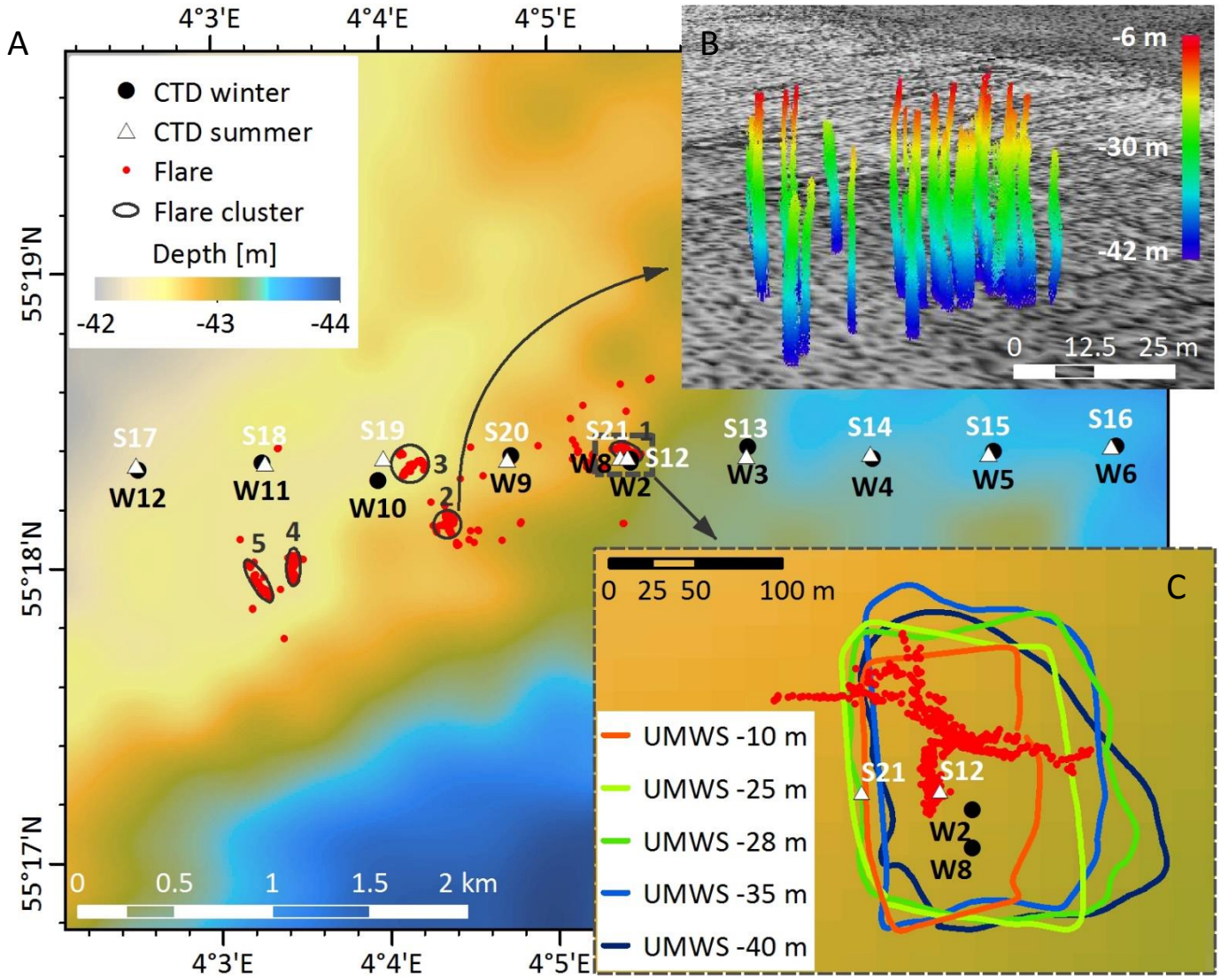


Fig. 2: A) Overview of gas flares mapped in January 2014 and CTD stations sampled in July 2013 (S12-S21) and January 2014 (W2-W12). Flares cluster in 5 distinct areas (cluster 1-5) and reach to 6 m from the sea surface (e.g. cluster 2 (B)), which corresponds to the echosounder's transducer depth. Hence, most likely the gas transport extends to the sea surface. Cluster 1 corresponds to the gas seep area investigated by Gentz (2013) (C).

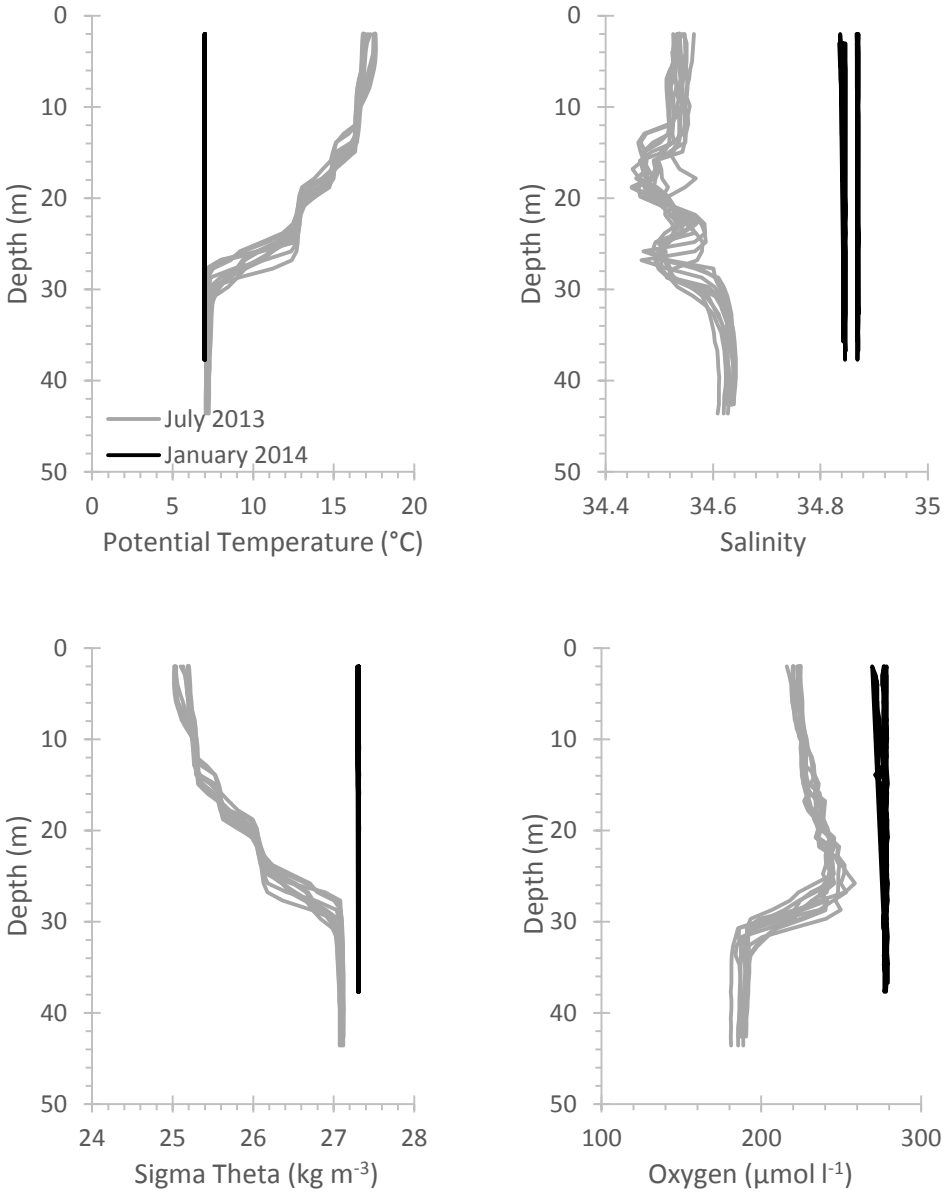


Fig. 3: Depth profiles of potential temperature, salinity, density (sigma theta), and oxygen for all stations in both summer and winter field programs.

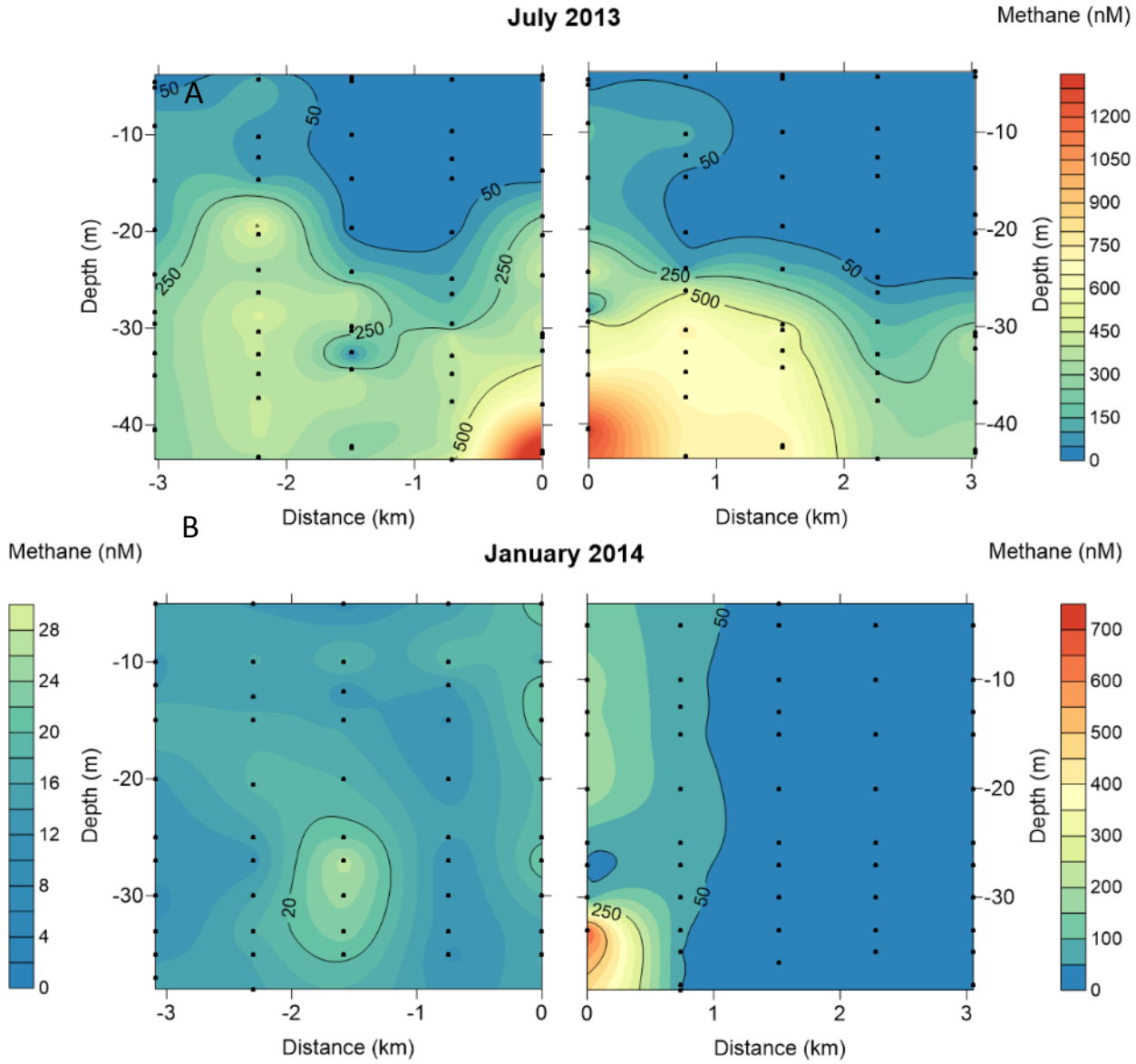


Fig. 4: A-B Contour plots of the dissolved methane concentrations measured in the water column in July 2013 and January 2014. The 6 km transect was divided into an eastern (positive numbers) and western part (negative numbers) starting from the center station at 0 km. Note the different methane concentration scales, which are necessary to properly display the different concentration ranges. The black dots indicate the sampled water depths.

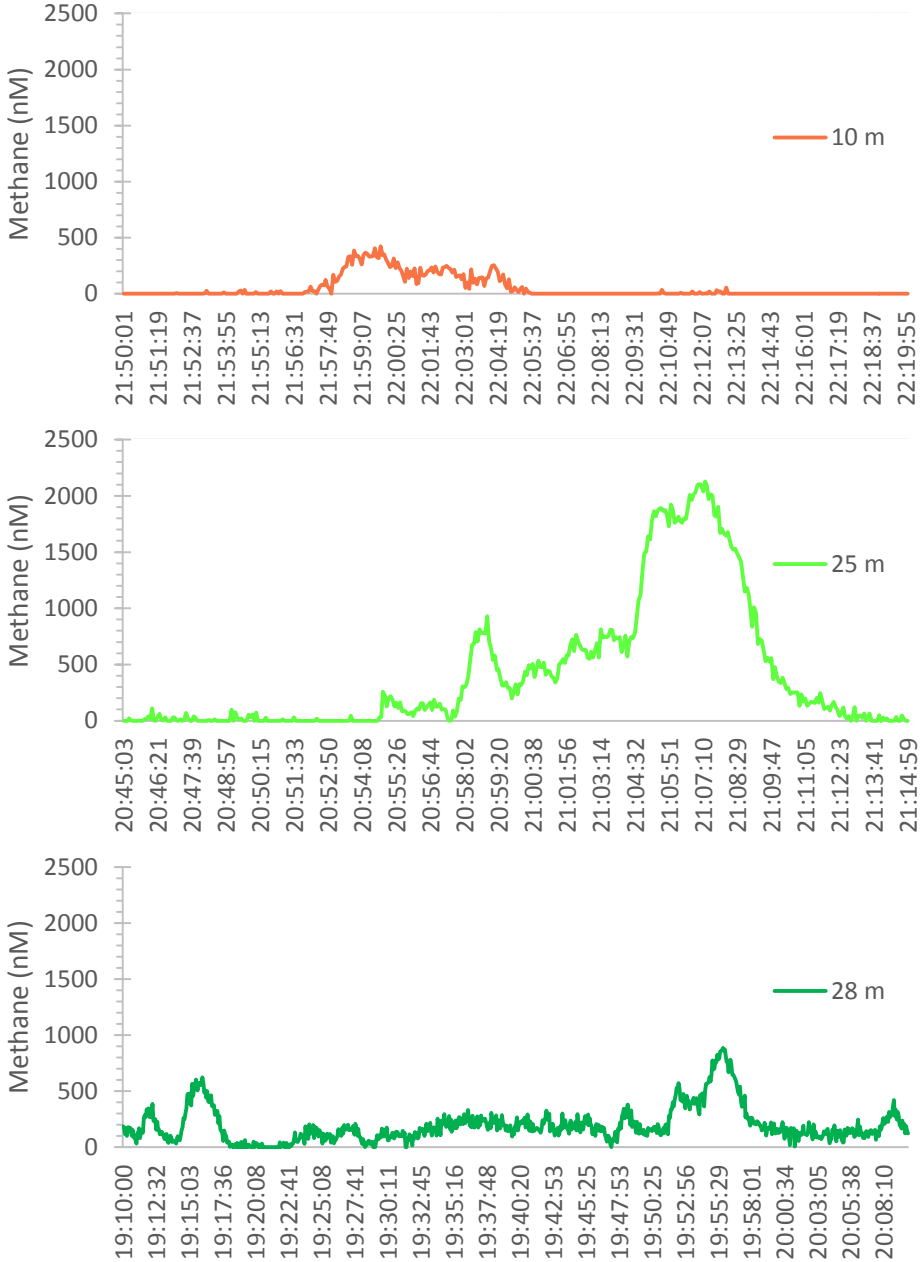


Fig. 5: Methane concentrations recorded by UWMS on 21.07.2013 in the vicinity of flare cluster 1 (Fig. 2C) at different water depth. The detection limit of the instrument is 16 nM, all measurements below this value are recorded as 0. Apart from temporal and spatial elevations most likely due to bubble streams, the background value is elevated throughout the recording time in 30 and 42 m water depth.

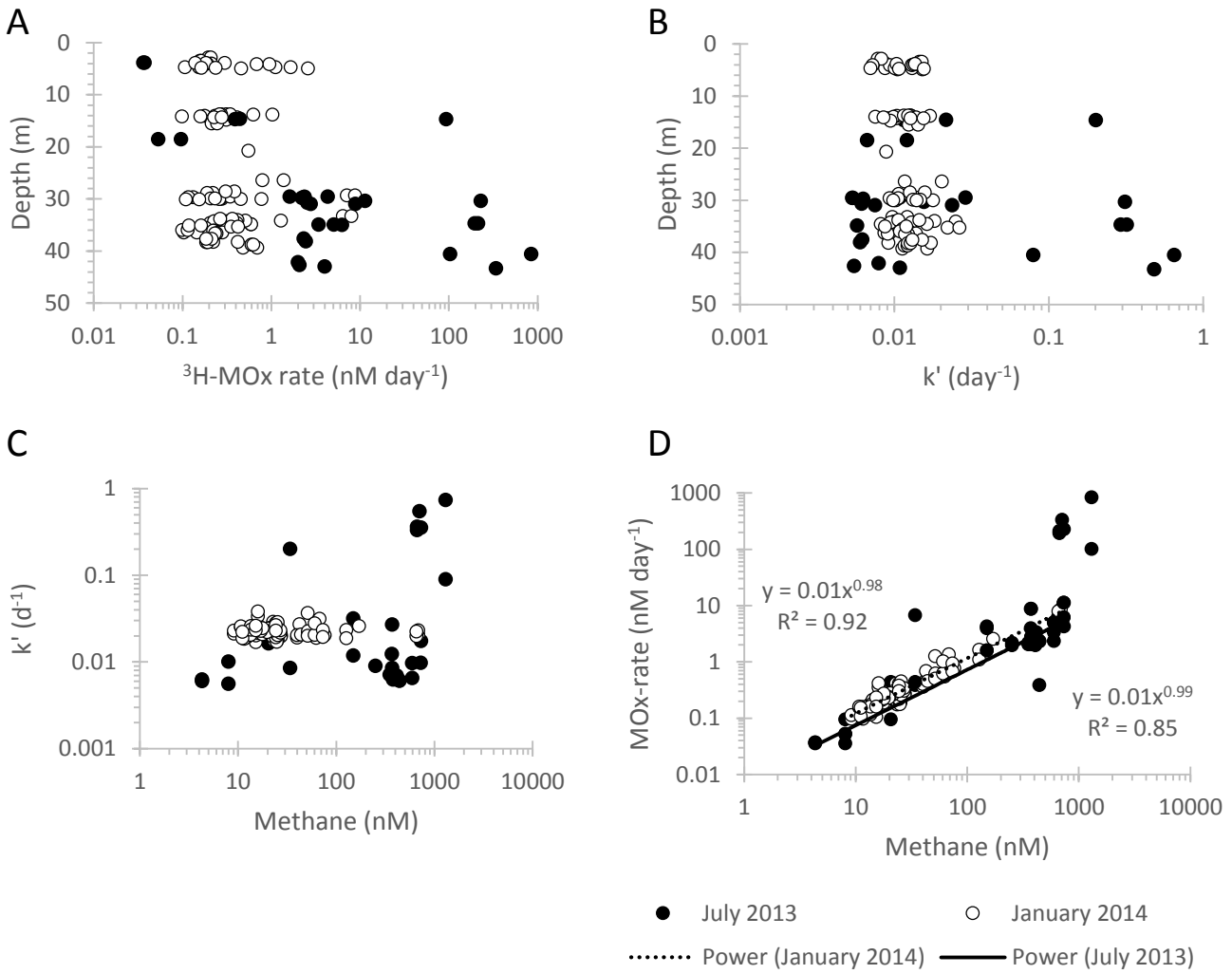


Fig. 6: Methane oxidation rates versus water depth measured with $^3$H-methane in July 2013 and in January 2014 (A). B The first order rate constant *k'* of summer and winter samples indicating the relative activity of the water. C *k'* versus methane concentration illustrate similar *k'* values over a wide range of methane concentration. D Methane oxidation rates versus methane concentrations shows for most of the data a first order function: $MOx=0.01[CH_4]^1$ (function with $R^2$ of 0.92 derived from winter data and with $R^2$ of 0.85 from summer data).

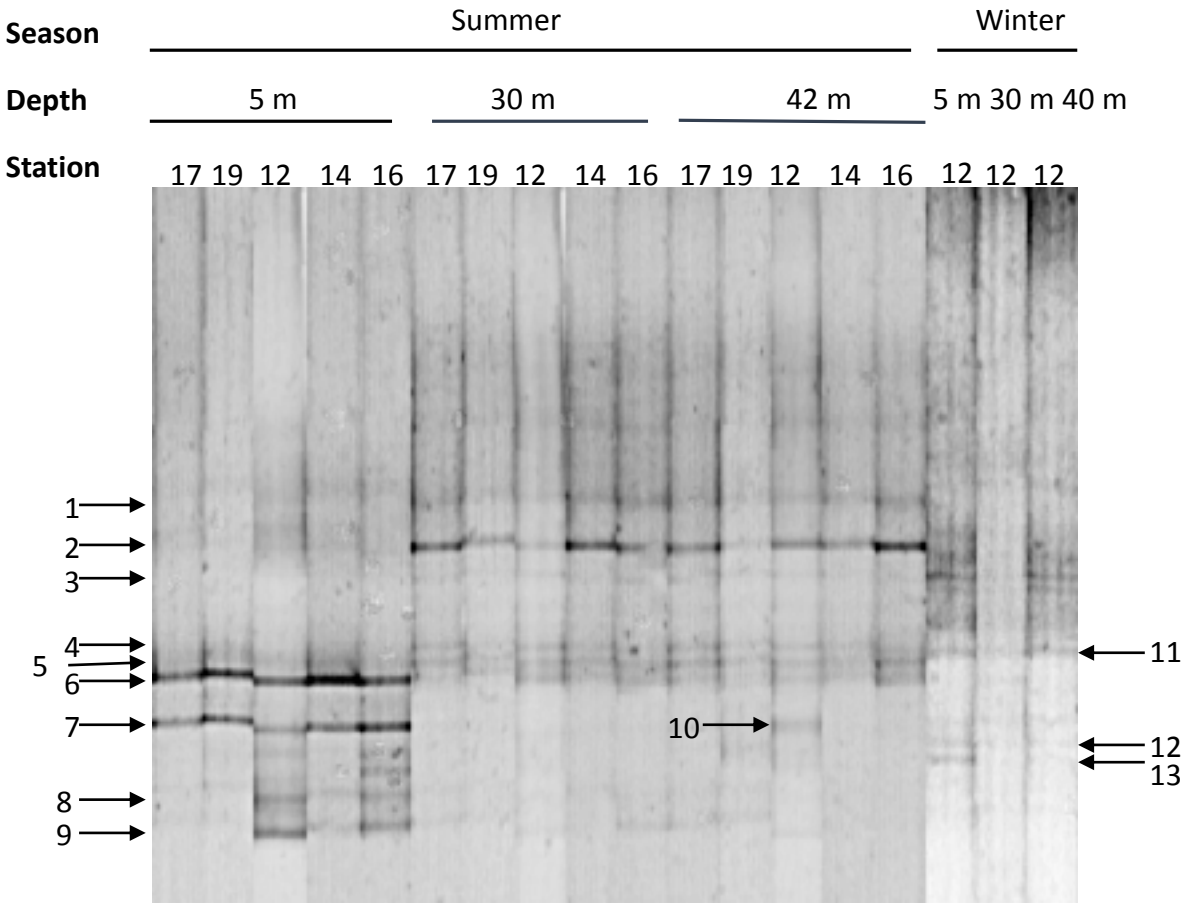


Fig. 7: DGGE profile of 16S rRNA gene fragments of samples from different depth and stations in the central North Sea. Numbers on the lines indicate excised and successfully sequenced DGGE bands, whose phylogenetic assignment is listed in Tab. 1.

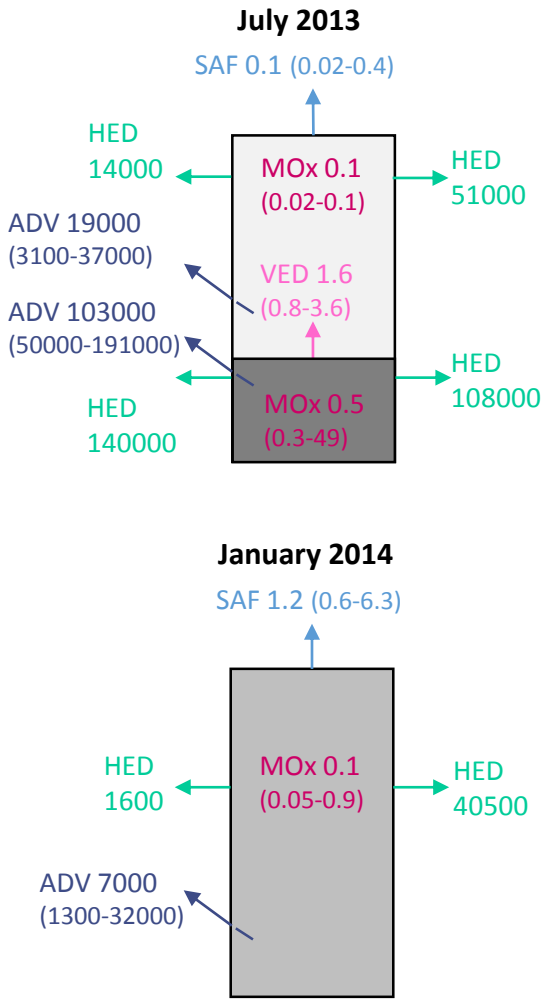


SAF – Sea Air Flux
MOx – Methane Oxidation rate
VED – Vertical Eddy Diffusion
HED – Horizontal Eddy Diffusion
ADV – Advection
Median of estimates (range of estimates)

Fig. 8: Sketch of transport and loss terms estimated for the study area in nmol $m^{-2}$ $s^{-1}$.